

# 3DGS-HPC: Distractor-free 3D Gaussian Splatting with Hybrid Patch-wise Classification

Jiahao Chen<sup>1,2</sup> Yipeng Qin<sup>3</sup> Ganlong Zhao<sup>4</sup> Xin Li<sup>2</sup> Wenping Wang<sup>2</sup> Guanbin Li<sup>1\*</sup>  
<sup>1</sup>Sun Yat-sen University <sup>2</sup>Texas A&M University <sup>3</sup>Cardiff University  
<sup>4</sup>Centre for Perceptual and Interactive Intelligence

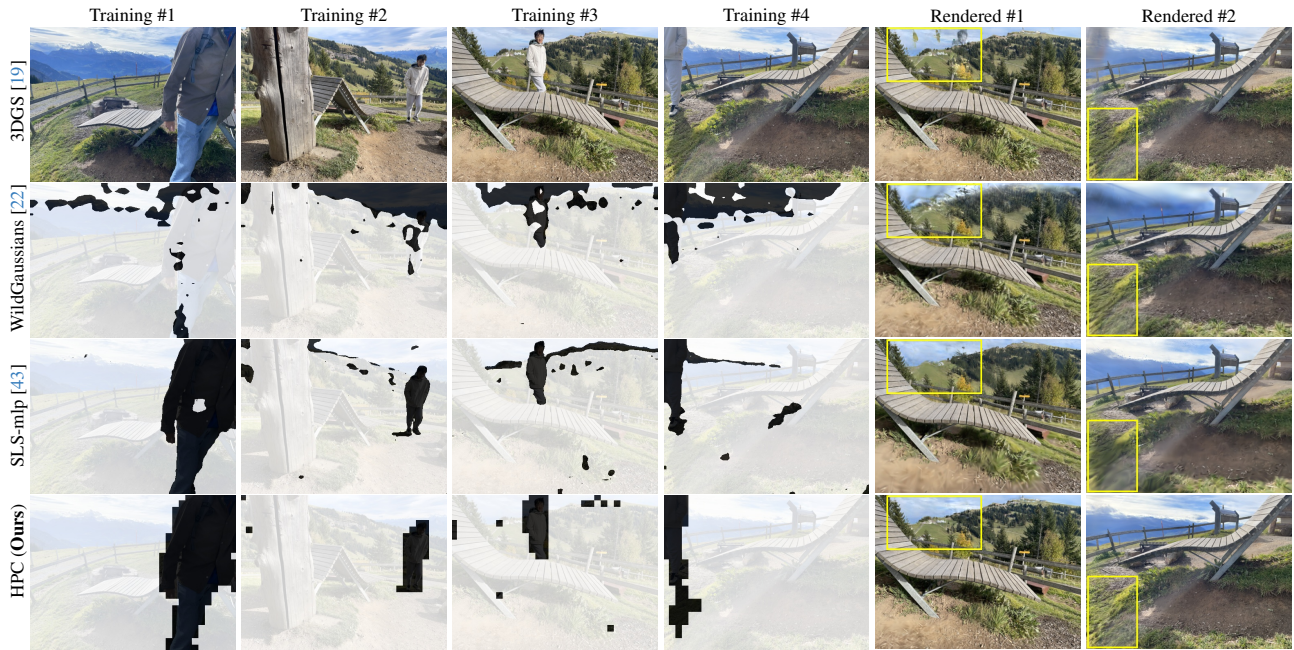


Figure 1. **Comparison between previous methods and our proposed Hybrid Patch-wise Classification (HPC).** When training 3DGS with static scenes disturbed by transient distractors, previous methods utilize image semantic priors but fail to separate transient distractors (e.g., pedestrians and shadows) from static backgrounds (e.g., mountains). By addressing their inherent semantic limitations, our method can generate binary masks that better represent transient distractors, thereby removing related artifacts in rendered results (yellow boxes).

## Abstract

3D Gaussian Splatting (3DGS) has demonstrated remarkable performance in novel view synthesis and 3D scene reconstruction, yet its quality often degrades in real-world environments due to transient distractors, such as moving objects and varying shadows. Existing methods commonly rely on semantic cues extracted from pre-trained vision models to identify and suppress these distractors, but such semantics are misaligned with the binary distinction between static and transient regions and remain fragile under the appearance perturbations introduced during 3DGS optimization. We propose 3DGS-HPC, a framework that

circumvents these limitations by combining two complementary principles: a patch-wise classification strategy that leverages local spatial consistency for robust region-level decisions, and a hybrid classification metric that adaptively integrates photometric and perceptual cues for more reliable separation. Extensive experiments demonstrate the superiority and robustness of our method in mitigating distractors to improve 3DGS-based novel view synthesis.

## 1. Introduction

Recent advances in 3D Gaussian Splatting (3DGS) [15, 17, 19, 20, 29, 63] have enabled high-quality novel view synthesis with real-time performance, establishing it as a strong

\*The corresponding author is Guanbin Li.

alternative to Neural Radiance Fields (NeRF) [34]. However, similar to NeRF, 3DGS is built upon the assumption that all training images capture a completely static scene. In real-world settings, this assumption is frequently violated by *transient distractors* (i.e., dynamic or temporally inconsistent elements such as pedestrians, vehicles, or shadows) that introduce artifacts and significantly degrade reconstruction quality. The diversity and unpredictability of these distractors in appearance, scale, and motion make them difficult to detect and remove reliably. As a result, transient distractors remain a key obstacle to deploying 3DGS for robust real-world scene reconstruction.

To mitigate the effects of distractors, most existing methods follow a simple yet effective paradigm: generating pixel-wise binary masks to label and filter out transient pixels in the training images, thereby preventing the model from being corrupted by distractors during optimization. This formulation reduces the task to estimating accurate binary masks, essentially a binary classification problem. Current research addresses this problem from two perspectives: *classification granularity* and *classification metric*. Early methods [10, 33, 42, 59] perform pixel-wise classification using photometric errors, but the resulting masks are often noisy and spatially inconsistent, as pixel-level predictions lack sufficient local context. Recent studies introduce semantic priors to improve both aspects. Some works [6, 22, 23, 37, 40, 43] enforce semantic coherence by unifying pixel-wise classification results into semantically consistent regions, thus enhancing spatial stability, while others [22, 32] adopt perceptual metrics that measure semantic similarity between training and rendered images. However, as shown in Fig. 1, semantic-coherence methods rely on external semantics derived from vision foundation models that are not explicitly designed to distinguish static from transient regions, resulting in a *semantic mismatch* between predicted and ground-truth transient areas. Perceptual metrics also suffer from *semantic fragility*, as their feature representations are highly sensitive to minor appearance perturbations, leading to unstable responses and the misclassification of static regions as transient.

In this work, we address the challenges of semantic mismatch and fragility in existing methods by introducing a novel framework for distractor-free 3DGS, termed *Hybrid Patch-wise Classification (HPC)*. From the perspective of classification granularity, HPC avoids reliance on semantics derived from unrelated tasks and instead leverages the assumption of *local spatial consistency*. By directly performing classification at the patch level, it captures richer local context than pixel-wise classification while maintaining higher robustness and efficiency than semantic region grouping. In terms of the classification metric, HPC integrates photometric and perceptual cues into a hybrid metric that adaptively balances color fidelity and semantic simi-

larity, yielding more reliable separation between static and transient regions. Extensive experiments demonstrate that HPC significantly improves the robustness and fidelity of 3DGS reconstructions in the presence of diverse distractors.

Our contributions are summarized as follows:

- We propose *Hybrid Patch-wise Classification (HPC)*, a novel framework for distractor-free 3D Gaussian Splatting (3DGS) that achieves robust reconstruction in real-world scenes containing transient distractors.
- To overcome the limitations of previous semantic-based methods, HPC introduces two complementary designs: a *patch-wise classification approach* that leverages local spatial consistency for efficient and context-aware classification, and a *hybrid classification metric* that adaptively fuses photometric and perceptual cues to enhance static/transient separation.
- We validate the effectiveness of HPC through extensive experiments, showing consistent improvements over state-of-the-art methods in both reconstruction quality and robustness to distractors.

## 2. Related Work

**NeRF & 3DGS in Non-static Scenes.** NeRF [34] has emerged as a promising solution to achieve high-quality 3D scene reconstruction and novel view synthesis, while 3DGS [19] has been proposed as a compelling alternative due to its real-time rendering speed and comparable rendering quality. However, both approaches and many of their variants assume that the scene to be reconstructed is static and are therefore not applicable to real-world scenes containing non-static elements. In contrast to methods that explicitly reconstruct dynamic components [14, 18, 26, 30, 57, 60, 61], our work follows another research line that treats these non-static elements as transient distractors and removes them to enhance the reconstruction of static content. Early attempts [28, 39, 44, 47, 48, 50] use pre-trained semantic segmentation models [7–9, 11] to detect transient distractors of known classes, but this prior information is intractable to obtain in practice. Subsequent research has focused on more generalizable approaches, which can be roughly grouped into two paradigms: uncertainty modeling [10, 13, 22, 23, 27, 32, 33, 37, 40, 53, 55, 59, 64], which relies on neural networks to predict pixel uncertainties of training images; and pixel classification [3, 6, 42, 43, 51, 54, 58], which directly classifies pixels as static or transient based on their reconstruction errors. We view the former as a soft form of the latter, as both rely on the Memorization Effect [1, 2, 46, 54] that neural networks tend to learn contextually consistent samples faster than inconsistent samples. Consequently, pixels with larger reconstruction errors or higher uncertainties are regarded as transient and excluded from optimization during training.

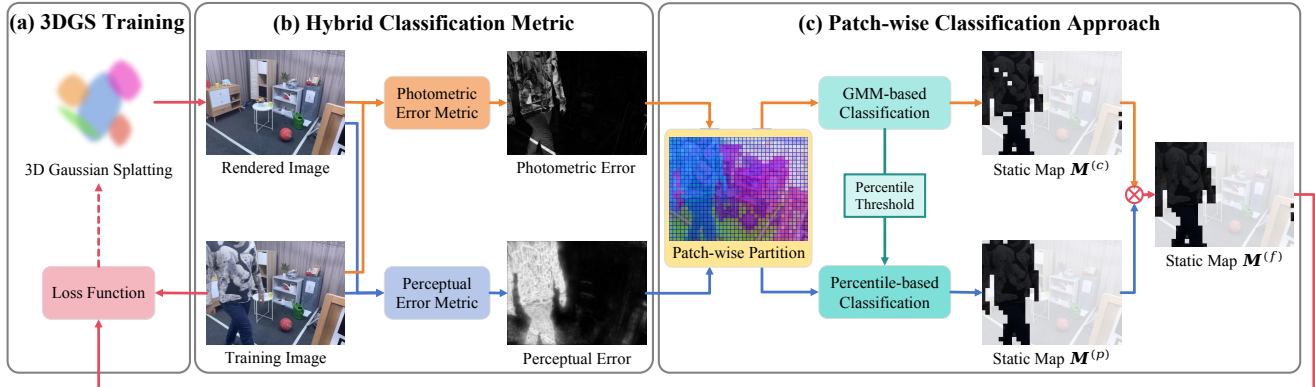


Figure 2. **Overview of Hybrid Patch-wise Classification (HPC).** Given training images disturbed by transient distractors, our method (a) optimizes 3D Gaussian Splatting following standard practice, (b) classifies static and transient regions using a novel hybrid metric that combines the strengths of photometric and perceptual cues, and (c) performs classification at the patch level to exploit local spatial consistency, thereby enhancing robustness and efficiency without relying on external semantics such as segmentation or detection models.

**Semantics in Distractor-free NeRF & 3DGS.** Recent advances in vision foundation models [5, 21, 36, 38, 41, 49] have inspired a new line of distractor-free NeRF and 3DGS methods that exploit semantic priors to better separate transient distractors from static backgrounds. These semantic priors are typically utilized in two ways:

- *Enhancing semantically coherent classification.* To encourage semantically similar pixels to produce coherent classification output, some methods [22, 32, 40, 43] incorporate image semantics as an auxiliary input to the prediction network, while others [6, 32, 37, 43] segment the image into semantically consistent regions and use this structure to refine classification results.
- *Serving as perceptual error metrics.* To address the limitations of photometric error metrics (*e.g.*, RGB L1 error, SSIM error) [6, 33, 40, 42] in distinguishing transient distractors from static content with similar colors or textures, recent studies [22, 32] adopt perceptual metrics derived from feature embeddings like DINOv2 [36] to capture semantic-level image differences.

Although these approaches achieve notable improvements, their reliance on external semantics introduces two challenges: *semantic mismatch* between general-purpose vision semantics and the specific static/transient distinction, and *semantic fragility* that small appearance perturbations may lead to unstable feature responses and misclassification. In our work, we address this gap by proposing a novel distractor-free 3DGS framework, which consists of i) a patch-wise classification approach that leverages local spatial consistency to improve robustness and efficiency without relying on external semantics, and ii) a hybrid classification metric that combines perceptual and photometric error cues to correct semantic perturbability.

### 3. Preliminaries

Given a set of multi-view images  $\mathcal{I} = \{\mathbf{I}_i \in \mathbb{R}^{H \times W \times 3}\}_{i=1}^{N_I}$  captured from a scene, we have:

**3D Gaussian Splatting (3DGS) [19].** 3DGS represents the scene as a set of learnable 3D Gaussians  $\mathcal{G} = \{\mathbf{g}_j\}_{j=1}^{N_G}$ , each characterized by its position, covariance, color coefficients, and opacity. Given the specific camera parameters  $\mathbf{P}_i$ , 3DGS render the corresponding image  $\hat{\mathbf{I}}_i$  in one forward pass instead of pixel batches like NeRF [34]:

$$\hat{\mathbf{I}}_i = F_{\text{render}}(\mathcal{G}, \mathbf{P}_i), \quad (1)$$

where  $F_{\text{render}}$  is the rendering function that performs 2D projection, tile splitting, depth-based sorting, and  $\alpha$ -blending. During training,  $\mathcal{G}$  is optimized by minimizing the photometric error between the rendered image  $\hat{\mathbf{I}}_i$  and the training image  $\mathbf{I}_i$  using the loss  $\mathcal{L}$  from the original paper [19]:

$$\mathcal{L}(\hat{\mathbf{I}}_i, \mathbf{I}_i) = (1 - \lambda)\mathcal{L}_1(\hat{\mathbf{I}}_i, \mathbf{I}_i) + \lambda\mathcal{L}_{\text{SSIM}}(\hat{\mathbf{I}}_i, \mathbf{I}_i), \quad (2)$$

where  $\lambda = 0.2$ , and  $\mathcal{L}_1$  and  $\mathcal{L}_{\text{SSIM}}$  are L1 loss and SSIM loss, respectively.

**3DGS in Non-static Scenes.** An effective strategy to avoid artifacts caused by transient distractors is to mask out pixels related to distractors (*i.e.*, transient pixels) during training. Following existing work [6, 42, 43], we introduce a binary map  $\mathbf{M}_i \in \{0, 1\}^{H \times W}$  for each image  $\mathbf{I}_i$ , where 1 indicates static pixels and 0 denotes transient ones. We then apply  $\mathbf{M}_i$  as masks to Eq. (2) to suppress distractor regions:

$$\mathcal{L}(\hat{\mathbf{I}}'_i, \mathbf{I}'_i) = (1 - \lambda)\mathcal{L}_1(\hat{\mathbf{I}}'_i, \mathbf{I}'_i) + \lambda\mathcal{L}_{\text{SSIM}}(\hat{\mathbf{I}}'_i, \mathbf{I}'_i), \quad (3)$$

where  $\hat{\mathbf{I}}'_i = \mathbf{M}_i \odot \hat{\mathbf{I}}_i$  and  $\mathbf{I}'_i = \mathbf{M}_i \odot \mathbf{I}_i$ . Thus, the quality of reconstruction critically depends on the accuracy of the binary maps, which our method aims to improve.

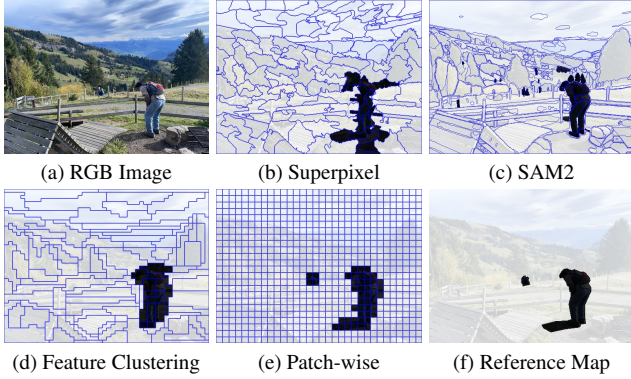


Figure 3. **Visualization of Different Partitioning Strategies.** When grouping pixels into multiple semantically consistent regions with blue borders, existing methods (b-d) fail to faithfully represent transient regions (*e.g.*, pedestrians and shadows) due to semantic mismatch between different tasks, while our patch-wise partition strategy (e) can accurately extract these regions.

## 4. Method

As Eq. (3) implies, the performance of the reconstruction model depends on the quality of binary maps, which are generated by classifying each pixel as static or transient. To this end, we propose a novel *Hybrid Patch-wise Classification (HPC)* framework (Fig. 2) that addresses the pixel classification challenge from two complementary perspectives: the classification approach (Sec. 4.1) and the classification metric (Sec. 4.2) as follows.

### 4.1. Patch-wise Classification Approach

Recent methods have increasingly focused on incorporating semantic consistency to refine noisy pixel-wise classification results by grouping pixels into regions with coherent internal semantics. This is typically achieved using superpixel algorithms [52], promptable object segmentation [21, 38], or semantic feature clustering [35, 49]. The motivation behind this trend stems from the observation that although static and transient pixels exhibit bimodal error distributions during training [42, 54], accurate separation remains difficult in practice due to the limited context at the pixel level, leading to sensitivity to local perturbations and inconsistent predictions. Despite their success, these methods overlook the subtle differences in semantics between distractor-free 3DGS and other tasks (*e.g.*, semantic segmentation), thus producing suboptimal results.

**Semantic Mismatch between Different Tasks.** As illustrated by the binary map in Eq. (3), distractor-free 3DGS requires only two semantic categories: static and transient. However, vision foundation models provide semantics optimized for general visual understanding rather than this binary separation, and no existing method can reliably extract these specific semantics. As a result, state-of-the-art approaches adopt workaround solutions by leveraging seman-

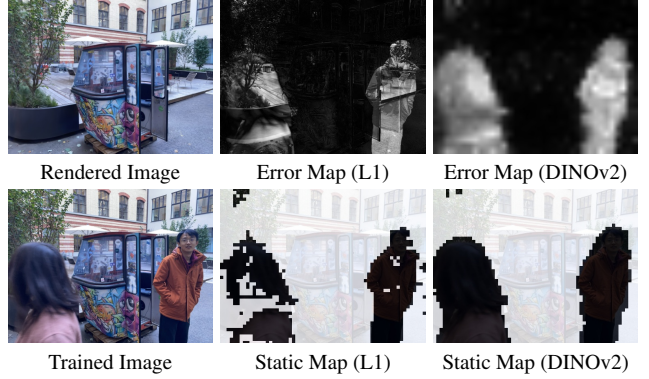


Figure 4. **Visualization of Different Error Metrics.** Given training images with distractors and corresponding rendered images, traditional photometric metrics (L1) produce noisy static maps due to low-level appearance ambiguities (*e.g.*, similar colors). Instead, perceptual metrics based on vision foundation models (DINOv2) produce clean static maps with clear boundaries.

tics defined for other tasks, under the assumption that static and transient regions can be approximated as a union of semantic regions for other tasks. For instance, as shown in Fig. 3, superpixel methods cluster pixels based on low-level appearance cues and are easily confused by color ambiguities (*e.g.*, black hairs *vs.* dark forests); SAM2 [38] segments objects via prompt-based priors and tends to overlook subtle transient cues (*e.g.*, merging human shadows into the same ground region); and feature clustering groups pixels by similarity in the embedding space of vision foundation models, which emphasizes semantic similarity rather than temporal or photometric consistency, resulting in misclassifications similar to those of SAM2. Although each provides a form of semantic partitioning, none of them faithfully captures the binary semantic distinction required for distractor-free 3DGS, leading to mismatches and reduced performance.

**Patch-wise Partition Strategy.** To bridge this gap, we propose a simple yet effective alternative that completely avoids external semantics. Instead of relying on task-specific semantic grouping, we leverage the assumption of *local spatial consistency* (*i.e.*, neighboring pixels within a small region tend to share the same property) to over-partition each training image into regular, non-overlapping patches and directly perform classification at the patch level. Patch-wise classification provides richer contextual cues than pixel-wise classification and greater robustness to local perturbations, while significantly reducing computational cost by aggregating pixels into fewer units to be classified. Although this mechanical partition may produce boundaries that do not align precisely with the edges of the object, existing work [32] has demonstrated that reconstruction quality remains largely unaffected, provided that transient distractors are effectively identified.

Concretely, given a pixel-wise error map  $\varepsilon_i \in \mathbb{R}^{H \times W}$

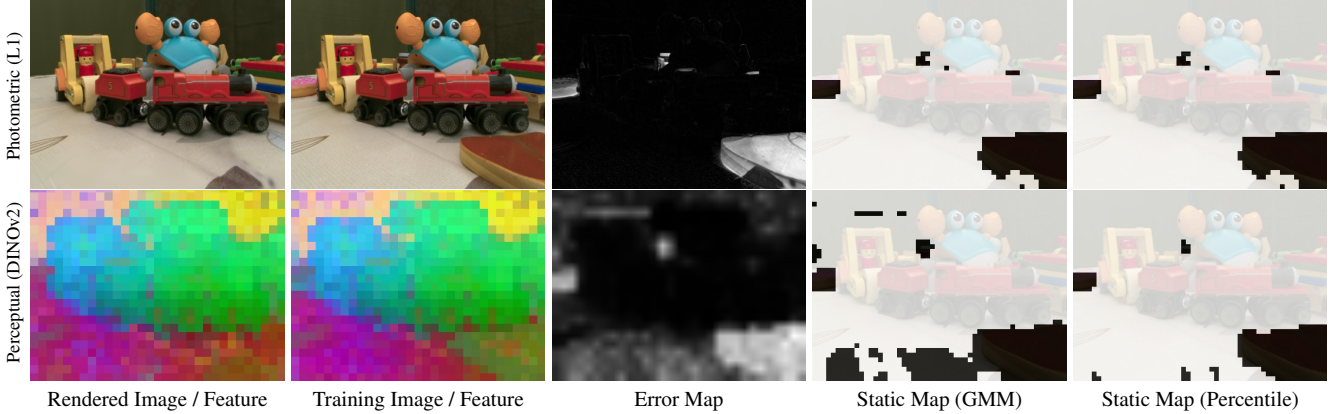


Figure 5. **Comparison of different classification approaches with different error metrics.** Bottom row: Although perceptual error metrics are effective in capturing semantic differences, they can produce anomalous results in textureless regions (*e.g.*, green wall and white tablecloth) due to visual perturbability (*e.g.*, blurring) between training and rendered images. Top row: In contrast, while inherently noisier, photometric error metrics demonstrate greater reliability in estimating the overall proportion of transient pixels within an image, thus guiding perception error metrics for more accurate classification.

for image  $\mathbf{I}_i$ , we reshape it into a sequence of non-overlapping patches  $\hat{\mathbf{e}}_i \in \mathbb{R}^{N_E \times P^2}$ , where  $(P, P)$  is the patch resolution and  $N_E = HW/P^2$  is the number of patches. The mean error of each patch forms a compact patch-wise error sequence  $\bar{\mathbf{e}}_i \in \mathbb{R}^{N_E}$  for classification.

**Classification Approaches (Percentile & GMM).** After aggregation, we can classify patches based on their total errors  $\mathcal{E} \in \mathbb{R}^{N_I \cdot N_E}$  using two approaches:

- *Percentile-based Classification.* If the static proportion  $\mathcal{T}$  of the scene is known, transient patches can be filtered using a percentile threshold:

$$\mathbf{M}_i(j) = \mathbb{I}[\bar{\mathbf{e}}_i(j) \leq \text{percentile}(\mathcal{E}, \mathcal{T})], \quad (4)$$

where  $\mathbf{M}_i(j)$  is the static mask of the  $j$ -th patch of the  $i$ -th image, and  $\mathbb{I}[\cdot]$  is the indicator function that returns 1 if the predicate is true and 0 otherwise.

- *GMM-based Classification.* In practice, the exact static proportion varies with different scenes and is hard to obtain in advance. To achieve accurate distinction in various settings, we follow prior works [24, 54] to fit the error distribution via a two-component one-dimensional Gaussian Mixture Model (GMM). The probability density function  $P(\bar{\mathbf{e}}_i(j))$  can be defined as:

$$P(\bar{\mathbf{e}}_i(j)) = \sum_{k=1}^2 \beta_k \cdot \mathcal{N}(\bar{\mathbf{e}}_i(j) \mid \mu_k, \sigma_k^2), \quad (5)$$

where  $\beta_k$  represents the mixing component of the  $k$ -th gaussian distribution  $\mathcal{N}(\cdot \mid \mu_k, \sigma_k^2)$  with the mean  $\mu_k$  and the variance  $\sigma_k^2$ . Let  $\mu_1 \leq \mu_2$ , we can view the first distribution as static, and then determine whether the  $j$ -th patch of the  $i$ -th image is static by the probability that its error value  $\bar{\mathbf{e}}_i(j)$  belongs to the static distribution:

$$\mathbf{M}_i(j) = \mathbb{I}\left[\frac{\beta_1 \cdot \mathcal{N}(\bar{\mathbf{e}}_i(j) \mid \mu_1, \sigma_1^2)}{\sum_{k=1}^2 \beta_k \cdot \mathcal{N}(\bar{\mathbf{e}}_i(j) \mid \mu_k, \sigma_k^2)} \geq 0.5\right]. \quad (6)$$

## 4.2. Hybrid Classification Metrics

While patch-wise classification improves spatial granularity and robustness, the effectiveness of distractor removal also depends on the reliability of the underlying classification metric. Recent state-of-the-art methods replace traditional photometric error metrics with perceptual error metrics (*e.g.*, DINOv2 [36]) to capture object-level inconsistencies between reference and rendered images. As shown in Fig. 4, these perceptual metrics offer clear advantages: they enable image comparison at the *semantic* level while exhibiting robustness to ambiguities at the *appearance* level (*e.g.*, objects with similar colors). Rather than contributing to this line of work by designing a better perceptual metric, our study takes a step back to critically examine the paradigm itself. Specifically, we identify an inherent limitation shared by existing perceptual metrics: *semantic fragility in specific image regions*. To address this challenge, we propose a novel hybrid classification metric that synergistically combines perceptual and photometric cues, leading to more robust and accurate static map construction.

**Semantic Fragility of Perceptual Metrics.** Despite their effectiveness, perceptual metrics can still yield anomalous results due to inconsistent semantic predictions of vision foundation models for minor appearance perturbations (*e.g.*, blurring or color jitter). Since feature extractors in these models are optimized for object-centric understanding rather than appearance consistency, their outputs are tuned to salient object-related features, leading to unstable activations in textureless regions. This issue is especially pronounced in low-frequency regions during 3DGS optimization, where appearance perturbations between train-

Method	Statue			Android			Yoda			Crab (2)			Avg.		
	PSNR↑	SSIM↑	LPIPS↓	PSNR↑	SSIM↑	LPIPS↓	PSNR↑	SSIM↑	LPIPS↓	PSNR↑	SSIM↑	LPIPS↓	PSNR↑	SSIM↑	LPIPS↓
RobustNeRF [42]	21.56	.841	.129	24.38	.828	.088	33.72	.940	.079	32.77	.934	.077	28.11	.886	.093
NeRF-HuGS [6]	22.14	.850	.120	24.40	.834	.088	33.64	.945	.057	33.83	.939	.061	28.50	.892	.081
NeRF On-the-go [40]	22.34	.849	.109	24.42	.823	.084	30.64	.933	.068	29.65	.917	.079	26.76	.881	.085
3DGS [19]	21.54	.848	.135	23.62	.814	.097	30.34	.945	.086	30.35	.944	.084	26.46	.888	.101
MemE-3DGS [54]	22.65	.851	.096	24.14	.810	.079	31.41	.928	.115	32.05	.940	.093	27.56	.882	.096
WildGaussians [22]	23.02	.861	.127	25.15	.837	.092	31.91	.944	.111	31.42	.936	.114	27.88	.894	.111
SLS-mlp [43]	22.81	.841	.119	25.04	.834	.079	35.52	.957	.071	34.66	.953	.076	29.51	.896	.086
HybridGS [27]	22.87	.862	.104	25.14	.848	.068	35.19	.958	.073	34.94	.955	.074	29.53	.906	.080
T-3DGS [32]	22.68	.855	.107	24.67	.822	.073	33.02	.942	.095	33.11	.943	.092	28.37	.890	.092
Ours (VGG)	23.04	.878	.096	25.12	.853	.064	35.78	.962	.068	35.43	.960	.066	29.84	.913	.074
Ours (ResNet)	23.09	.879	.095	25.01	.851	.065	35.88	.962	.068	35.49	.960	.066	29.87	.913	.073
Ours (DINOv2)	23.38	.880	.094	25.02	.851	.065	35.79	.962	.068	35.07	.957	.071	29.81	.913	.074

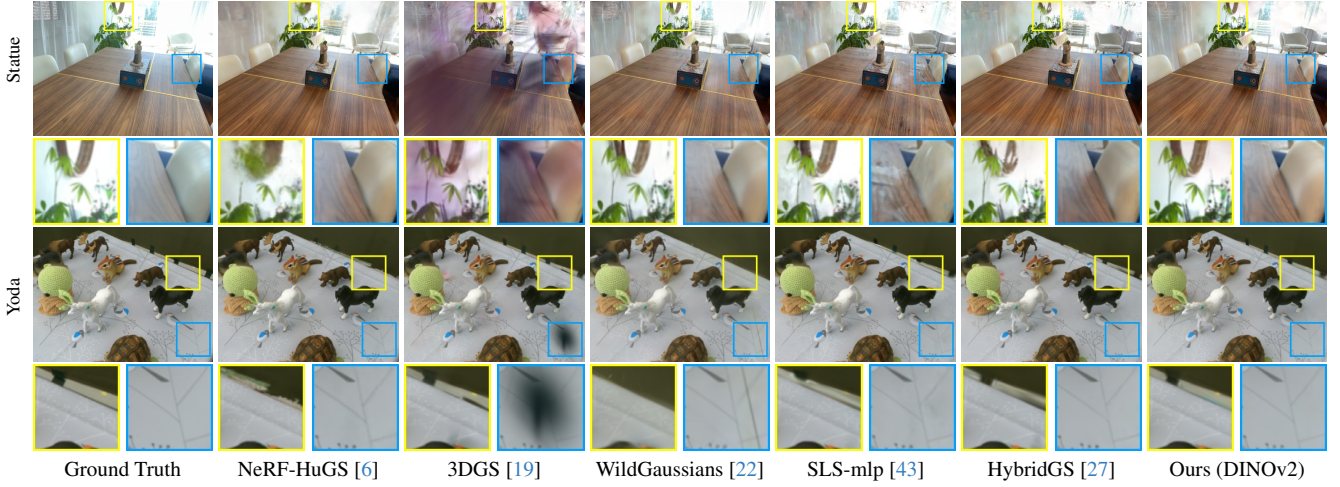


Figure 6. **Quantitative and Qualitative Comparisons on the RobustNeRF Dataset [42].** The first, second, and third best values are highlighted. Quantitatively, our method with different vision models not only improves the performance of native 3DGS, but also outperforms previous methods on most quality metrics. Qualitatively, our method can better preserve static details while ignoring distractors.

ing and predicted images can dominate and result in abnormally high perceptual errors, causing static areas to be incorrectly classified as transient (Fig. 5). Given that low-texture regions constitute a significant portion of natural images [4, 12, 25, 31], perceptual metrics are therefore inherently prone to erroneously filter out a greater number of static regions compared to their photometric counterparts.

**Hybrid Metric Formulation.** We therefore propose a hybrid classification metric that combines perceptual and photometric cues. In this framework, the photometric error (processed via GMM-based classification) provides an estimated static pixel proportion, which guides the percentile thresholding used in perceptual error-based classification. By jointly measuring image differences in both color and semantic spaces, this hybrid approach not only improves classification accuracy but also enables adaptive control over the static proportion within a reasonable range.

Specifically, we first obtain the photometric error map  $\varepsilon_i^{(c)}$  and the perceptual error map  $\varepsilon_i^{(p)}$  between the rendered image  $\hat{\mathbf{I}}_i$  and the training image  $\mathbf{I}_i$  by using the RGB L1

loss and the feature cosine similarity loss, respectively:

$$\varepsilon_i^{(c)} = \|\hat{\mathbf{I}}_i - \mathbf{I}_i\|_1, \quad (7)$$

$$\varepsilon_i^{(p)} = 1 - \frac{\hat{\mathbf{f}}_i \cdot \mathbf{f}_i}{\|\hat{\mathbf{f}}_i\|_2 \cdot \|\mathbf{f}_i\|_2}, \quad (8)$$

where  $\hat{\mathbf{f}}_i$  and  $\mathbf{f}_i$  are feature maps extracted from vision foundation models. We follow the process in Sec. 4.1 to reorganize photometric error maps into the patch-wise error sequence, and then classify it through Eq. (6) to obtain the static map  $\mathbf{M}_i^{(c)}$  and the estimated static proportion  $\mathcal{T}^{(c)}$ :

$$\mathcal{T}^{(c)} = \frac{\sum_{i=1}^{N_I} \sum_{j=1}^{N_E} \mathbf{M}_i^{(c)}(j)}{N_I \cdot N_E}. \quad (9)$$

Similarly, we reorganize the perceptual error maps and obtain their static map  $\mathbf{M}_i^{(p)}$  through Eq. (4) with  $\mathcal{T}^{(c)}$ . The final static map  $\mathbf{M}_i^{(f)}$  can be defined as:

$$\mathbf{M}_i^{(f)} = \mathbf{M}_i^{(c)} \cap \mathbf{M}_i^{(p)}. \quad (10)$$

In the end, the static map  $\mathbf{M}_i^{(f)}$  is applied to Eq. (3) to filter out transient distractors during training.

Method	Low Occlusion						Medium Occlusion						High Occlusion						Avg.		
	Mountain		Fountain		Patio		Corner		Spot		Patio-High		Avg.		Avg.						
	PSNR↑	SSIM↑	LPIPS↓	PSNR↑	SSIM↑	LPIPS↓	PSNR↑	SSIM↑	LPIPS↓	PSNR↑	SSIM↑	LPIPS↓	PSNR↑	SSIM↑	LPIPS↓	PSNR↑	SSIM↑	LPIPS↓			
RobustNeRF [42]	21.37	.732	.151	20.97	.717	.191	24.30	.863	.099	21.33	.781	.127	21.83	.686	.372	19.78	.632	.317	21.60	.735	.210
NeRF-HuGS [6]	21.65	.741	.148	21.44	.732	.174	26.52	.879	.087	22.06	.812	.108	23.06	.823	.157	22.45	.776	.173	22.86	.794	.141
NeRF On-the-go [40]	21.27	.719	.148	16.11	.482	.429	25.96	.865	.086	21.47	.793	.117	24.06	.865	.088	22.25	.790	.158	21.85	.752	.171
3DGS [19]	20.79	.749	.153	21.27	.773	.157	22.77	.832	.154	17.66	.715	.204	18.60	.737	.389	18.09	.701	.296	19.86	.751	.225
MemE-3DGS [54]	20.45	.699	.173	21.70	.744	.152	25.26	.867	.081	16.81	.728	.183	23.68	.880	.121	20.68	.764	.187	21.43	.780	.149
WildGaussians [22]	20.57	.706	.224	22.33	.757	.180	26.13	.881	.102	21.82	.823	.126	24.96	.867	.121	23.29	.814	.157	23.18	.808	.152
SLS-mlp [43]	21.99	.726	.189	22.48	.760	.168	26.33	.889	.090	22.50	.828	.108	24.34	.855	.132	23.15	.805	.152	23.47	.810	.140
HybridGS [27]	21.26	.618	.348	20.68	.631	.251	24.84	.817	.119	21.90	.784	.149	23.81	.712	.191	21.59	.689	.216	22.35	.708	.212
T-3DGS [32]	20.50	.689	.195	22.45	.770	.137	25.50	.870	.081	21.99	.842	.094	24.83	.887	.116	22.43	.806	.147	22.95	.811	.128
Ours (VGG)	21.64	.778	.134	23.31	.812	.121	25.18	.898	.082	22.69	.846	.096	24.99	.902	.091	23.54	.851	.120	23.56	.848	.107
Ours (ResNet)	22.40	.786	.128	23.58	.815	.117	25.44	.899	.079	22.64	.846	.094	25.75	.904	.090	23.17	.851	.120	23.83	.850	.105
Ours (DINOv2)	22.20	.784	.129	23.40	.813	.117	25.72	.900	.077	22.67	.845	.095	25.83	.899	.096	23.36	.850	.122	23.86	.849	.106



Figure 7. **Quantitative and Qualitative Comparisons on the On-the-go Dataset [40].** The first, second, and third best values are highlighted. Our method consistently achieves top-three quantitative results in scenes with varying ratios of transient distractors. In terms of visual quality, our method can better reconstruct static content, while previous methods suffer from missing or distorted details.

## 5. Experiments

### 5.1. Experimental Setups

**Datasets.** We use two public datasets in our experiments:

- *RobustNeRF Dataset [42].* This real-world dataset includes 4 controlled indoor scenes, each with 1-150 common objects placed as distractors. Following the baseline settings, we report results on the latest version [43] and downsample images by 8x for training and evaluation.
- *On-the-go Dataset [40].* This real-world dataset contains multiple casually captured indoor and outdoor scenes, each with varying ratios of distractors (from 5% to over 30%). Following the baseline settings, we report results on the 6 selected scenes representing different occlusion rates, and downsample images by 8x for training and evaluation (except images of *Patio* downsampled by 4x).

**Implementation Details.** Please see the supplementary materials for more details. In short, we develop our method based on open-source gsplat [62], and follow the same model architecture and training strategies as native 3DGS [19], except that a modified loss Eq. (3) is applied to filter out distractors. We warm up the model without applying static maps in the first 500 iterations and then update static maps every 100 iterations. For patch-wise classification approaches, we set the patch size to 16 by default. For perceptual error metrics, we separately apply three vision foundation models with different architectures: VGG16 [45], ResNet18 [16], and DINOv2 ViT-S/14 [36].

### 5.2. Evaluation on Novel View Synthesis

**Baselines.** In addition to native 3DGS, we compare our method to three state-of-the-art NeRF-based methods and five recent 3DGS-based methods: RobustNeRF [42],

Partition	RobustNeRF (Avg.)			On-the-go (Avg.)		
	PSNR $\uparrow$	SSIM $\uparrow$	LPIPS $\downarrow$	PSNR $\uparrow$	SSIM $\uparrow$	LPIPS $\downarrow$
(a) N/A	29.67	.911	.077	22.95	.834	.127
(b) Superpixel [52]	29.74	.912	.075	23.29	.846	.109
(c) SAM2 [38]	29.45	.913	.074	23.19	.844	.112
(d) Feat. Clustering [49]	29.70	.912	.075	23.71	.848	.107
(e) Patch-wise (Ours)	29.81	.913	.074	23.86	.849	.106

Figure 8. **Comparisons of Partitioning Strategies.** Pixel-wise method (a) produces noisy static maps, while other methods (b-d) confuse the desktop with transient shadows. Instead, our method (e) accurately distinguishes between transient and static elements.

NeRF-HuGS [6], NeRF On-the-go [40], MemE-3DGS [54], WildGaussians [22], SLS-mlp [43], HybridGS [27], and T-3DGS [32]. Among them, NeRF-HuGS, NeRF On-the-go, WildGaussians, SLS-mlp and T-3DGS utilize the semantic priors [21, 36, 41] to enhance the semantic consistency of the results, while WildGaussians and T-3DGS additionally use DINOv2 cosine error as a perceptual metric. The above models and ours are trained on images disturbed by distractors and evaluated on clean images. We report image synthesis quality based on PSNR, SSIM [56] and LPIPS [65].

**Comparisons on the RobustNeRF dataset (Fig. 6).** Compared to native 3DGS, applying our method leads to substantial PSNR improvements of 1.39 to 5.54 dB, indicating that our method can generate high-quality static maps to prevent native 3DGS from being affected by transient distractors. Compared to other baselines, our method achieves almost all the best quantitative results and maintains a good balance between ignoring transient distractors (*e.g.*, pink and dark artifacts) and preserving static details (*e.g.*, the mirror and wall structure). Furthermore, our method does not show significant performance differences when using different vision foundation models, demonstrating the adaptability and generalizability of our method.

**Comparisons on the On-the-go dataset (Fig. 7).** The results and conclusions are similar to those from the RobustNeRF dataset. Specifically, even with semantic priors, WildGaussians and SLS-mlp still fail to eliminate distractors (*e.g.*, temporal shadows) while incorrectly losing static details (*e.g.*, ground textures and the bicycle frame). Instead, our method achieves better visual quality by addressing inherent mismatches and biases in external semantics to better separate transient distractors from static background.

### 5.3. Ablation Study

Based on our method with DINOv2, we test two key components to study their effects on different datasets. More

	Photometric	Perceptual	Avg. Static%	RobustNeRF (Avg.)			On-the-go (Avg.)		
				PSNR $\uparrow$	SSIM $\uparrow$	LPIPS $\downarrow$	PSNR $\uparrow$	SSIM $\uparrow$	LPIPS $\downarrow$
(a)	GMM	-	85.31	29.82	.912	.074	22.83	.835	.123
(b)	-	GMM	73.22	29.13	.905	.085	23.40	.834	.129
(c)	-	Percentile	86.26	29.55	.912	.074	23.31	.845	.116
(d)	GMM	GMM	72.62	29.48	.909	.083	23.06	.825	.135
(e)	GMM	Percentile	82.75	29.81	.913	.074	23.86	.849	.106

Figure 9. **Comparisons of Classification Metrics.** Method (a) fails to distinguish distractors (*e.g.*, clothing) that closely resemble static backgrounds in color space, while Method (b) tends to incorrectly remove certain static regions (*e.g.*, wall surfaces). A naive combination (d) does not yield meaningful improvements. In contrast, our method (e) effectively separates transient distractors from the static background.

experiments and related analyzes can be found in the supplementary material.

**Partitioning Strategies.** As shown in Fig. 8, method (a) without any partitioning strategy performs the worst. Methods (b-d) rely on low-level appearance cues or deep semantic priors to organize pixels, achieving suboptimal results. In contrast, our method (e) performs the best, indicating that the simple patch-wise strategy is sufficient for this task.

**Classification Metrics.** As shown in Fig. 9, using perceptual metrics alone (b) performs worse than using color metrics alone (a) in some cases, and their difference in estimated static proportions is aligned with the analysis of Sec. 4.2. Method (d), which simply combines them, cannot achieve better performance. By using the static proportion estimated by color metrics to guide perceptual metrics for classification, our method (e) achieves the best results.

## 6. Conclusion

In conclusion, we presented Hybrid Patch-wise Classification (HPC), a novel framework for enabling distractor-free 3D Gaussian Splatting. By combining a patch-wise classification strategy with a hybrid error metric that fuses perceptual and color cues, our method effectively addresses the limitations of existing approaches that rely on mismatched external semantics. Extensive experiments demonstrate that HPC significantly improves reconstruction quality and robustness in the presence of transient distractors, offering a practical and generalizable solution for real-world 3DGS applications. Please see the supplementary details for **limitations and future work**.

## References

- [1] Eric Arazo, Diego Ortego, Paul Albert, Noel O’Connor, and Kevin McGuinness. Unsupervised label noise modeling and

- loss correction. In *International conference on machine learning*, pages 312–321. PMLR, 2019. 2
- [2] Devansh Arpit, Stanisław Jastrzębski, Nicolas Ballas, David Krueger, Emmanuel Bengio, Maxinder S Kanwal, Tegan Maharaj, Asja Fischer, Aaron Courville, Yoshua Bengio, et al. A closer look at memorization in deep networks. In *International conference on machine learning*, pages 233–242. PMLR, 2017. 2
- [3] Yanqi Bao, Jing Liao, Jing Huo, and Yang Gao. Distractor-free generalizable 3d gaussian splatting. *arXiv preprint arXiv:2411.17605*, 2024. 2
- [4] Robert W Buccirossi and Eero P Simoncelli. Image compression via joint statistical characterization in the wavelet domain. *IEEE transactions on Image processing*, 8(12): 1688–1701, 1999. 6
- [5] Mathilde Caron, Hugo Touvron, Ishan Misra, Hervé Jégou, Julien Mairal, Piotr Bojanowski, and Armand Joulin. Emerging properties in self-supervised vision transformers. In *Proceedings of the IEEE/CVF international conference on computer vision*, pages 9650–9660, 2021. 3
- [6] Jiahao Chen, Yipeng Qin, Lingjie Liu, Jiangbo Lu, and Guanbin Li. Nerf-hugs: Improved neural radiance fields in non-static scenes using heuristics-guided segmentation. In *Proceedings of the IEEE/CVF Conference on Computer Vision and Pattern Recognition*, pages 19436–19446, 2024. 2, 3, 6, 7, 8, 1
- [7] Liang-Chieh Chen, George Papandreou, Iasonas Kokkinos, Kevin Murphy, and Alan L Yuille. Deeplab: Semantic image segmentation with deep convolutional nets, atrous convolution, and fully connected crfs. *IEEE transactions on pattern analysis and machine intelligence*, 40(4):834–848, 2017. 2
- [8] Liang-Chieh Chen, George Papandreou, Florian Schroff, and Hartwig Adam. Rethinking atrous convolution for semantic image segmentation. *arXiv preprint arXiv:1706.05587*, 2017.
- [9] Liang-Chieh Chen, Yukun Zhu, George Papandreou, Florian Schroff, and Hartwig Adam. Encoder-decoder with atrous separable convolution for semantic image segmentation. In *Proceedings of the European conference on computer vision (ECCV)*, pages 801–818, 2018. 2
- [10] Xingyu Chen, Qi Zhang, Xiaoyu Li, Yue Chen, Ying Feng, Xuan Wang, and Jue Wang. Hallucinated neural radiance fields in the wild. In *Proceedings of the IEEE/CVF Conference on Computer Vision and Pattern Recognition*, pages 12943–12952, 2022. 2
- [11] Bowen Cheng, Ishan Misra, Alexander G Schwing, Alexander Kirillov, and Rohit Girdhar. Masked-attention mask transformer for universal image segmentation. In *Proceedings of the IEEE/CVF conference on computer vision and pattern recognition*, pages 1290–1299, 2022. 2
- [12] Taeg Sang Cho, Neel Joshi, C Lawrence Zitnick, Sing Bing Kang, Richard Szeliski, and William T Freeman. A content-aware image prior. In *2010 IEEE Computer Society Conference on Computer Vision and Pattern Recognition*, pages 169–176. IEEE, 2010. 6
- [13] Hiba Dahmani, Moussab Bennehar, Nathan Piasco, Luis Roldao, and Dzmityr Tsishkou. Swag: Splatting in the wild images with appearance-conditioned gaussians. In *European Conference on Computer Vision*, pages 325–340. Springer, 2024. 2
- [14] Yuanxing Duan, Fangyin Wei, Qiyu Dai, Yuhang He, Wenzheng Chen, and Baoquan Chen. 4d-rotor gaussian splatting: towards efficient novel view synthesis for dynamic scenes. In *ACM SIGGRAPH 2024 Conference Papers*, pages 1–11, 2024. 2
- [15] Antoine Guédon and Vincent Lepetit. Sugar: Surface-aligned gaussian splatting for efficient 3d mesh reconstruction and high-quality mesh rendering. In *Proceedings of the IEEE/CVF Conference on Computer Vision and Pattern Recognition*, pages 5354–5363, 2024. 1
- [16] Kaiming He, Xiangyu Zhang, Shaoqing Ren, and Jian Sun. Deep residual learning for image recognition. In *Proceedings of the IEEE conference on computer vision and pattern recognition*, pages 770–778, 2016. 7, 1
- [17] Binbin Huang, Zehao Yu, Anpei Chen, Andreas Geiger, and Shenghua Gao. 2d gaussian splatting for geometrically accurate radiance fields. In *ACM SIGGRAPH 2024 conference papers*, pages 1–11, 2024. 1
- [18] Nan Huang, Xiaobao Wei, Wenzhao Zheng, Pengju An, Ming Lu, Wei Zhan, Masayoshi Tomizuka, Kurt Keutzer, and Shanghang Zhang. S3gaussian: Self-supervised street gaussians for autonomous driving. *arXiv preprint arXiv:2405.20323*, 2024. 2
- [19] Bernhard Kerbl, Georgios Kopanas, Thomas Leimkühler, and George Drettakis. 3d gaussian splatting for real-time radiance field rendering. *ACM Transactions on Graphics*, 42(4):1–14, 2023. 1, 2, 3, 6, 7, 5
- [20] Shakiba Kheradmand, Daniel Rebain, Gopal Sharma, Weiwei Sun, Yang-Che Tseng, Hossam Isack, Abhishek Kar, Andrea Tagliasacchi, and Kwang Moo Yi. 3d gaussian splatting as markov chain monte carlo. *Advances in Neural Information Processing Systems*, 37:80965–80986, 2024. 1
- [21] Alexander Kirillov, Eric Mintun, Nikhila Ravi, Hanzi Mao, Chloe Rolland, Laura Gustafson, Tete Xiao, Spencer Whitehead, Alexander C Berg, Wan-Yen Lo, et al. Segment anything. In *Proceedings of the IEEE/CVF international conference on computer vision*, pages 4015–4026, 2023. 3, 4, 8, 1
- [22] Jonas Kulhanek, Songyou Peng, Zuzana Kukelova, Marc Pollefeys, and Torsten Sattler. Wildgaussians: 3d gaussian splatting in the wild. *arXiv preprint arXiv:2407.08447*, 2024. 1, 2, 3, 6, 7, 8, 5
- [23] Jaewon Lee, Injae Kim, Hwan Heo, and Hyunwoo J Kim. Semantic-aware occlusion filtering neural radiance fields in the wild. *arXiv preprint arXiv:2303.03966*, 2023. 2
- [24] Junnan Li, Richard Socher, and Steven CH Hoi. Dividemix: Learning with noisy labels as semi-supervised learning. *arXiv preprint arXiv:2002.07394*, 2020. 5
- [25] Xin Li and Michael T Orchard. New edge-directed interpolation. *IEEE transactions on image processing*, 10(10): 1521–1527, 2001. 6
- [26] Zhan Li, Zhang Chen, Zhong Li, and Yi Xu. Spacetime gaussian feature splatting for real-time dynamic view synthesis. In *Proceedings of the IEEE/CVF Conference on Computer Vision and Pattern Recognition*, pages 8508–8520, 2024. 2

- [27] Jingyu Lin, Jiaqi Gu, Lubin Fan, Bojian Wu, Yujing Lou, Renjie Chen, Ligang Liu, and Jieping Ye. Hybrids: Decoupling transients and statics with 2d and 3d gaussian splatting. *arXiv preprint arXiv:2412.03844*, 2024. 2, 6, 7, 8, 5
- [28] Yu-Lun Liu, Chen Gao, Andreas Meuleman, Hung-Yu Tseng, Ayush Saraf, Changil Kim, Yung-Yu Chuang, Johannes Kopf, and Jia-Bin Huang. Robust dynamic radiance fields. In *Proceedings of the IEEE/CVF Conference on Computer Vision and Pattern Recognition*, pages 13–23, 2023. 2
- [29] Tao Lu, Mulin Yu, Linning Xu, Yuanbo Xiangli, Limin Wang, Dahua Lin, and Bo Dai. Scaffold-gs: Structured 3d gaussians for view-adaptive rendering. In *Proceedings of the IEEE/CVF Conference on Computer Vision and Pattern Recognition*, pages 20654–20664, 2024. 1
- [30] Jonathon Luiten, Georgios Kopanas, Bastian Leibe, and Deva Ramanan. Dynamic 3d gaussians: Tracking by persistent dynamic view synthesis. In *2024 International Conference on 3D Vision (3DV)*, pages 800–809. IEEE, 2024. 2
- [31] Siwei Lyu. Automatic image orientation determination with natural image statistics. In *Proceedings of the 13th annual ACM international conference on Multimedia*, pages 491–494, 2005. 6
- [32] Alexander Markin, Vadim Pryadilshchikov, Artem Komarichev, Ruslan Rakhimov, Peter Wonka, and Evgeny Burnaev. T-3dgs: Removing transient objects for 3d scene reconstruction. *arXiv preprint arXiv:2412.00155*, 2024. 2, 3, 4, 6, 7, 8, 1, 5
- [33] Ricardo Martin-Brualla, Noha Radwan, Mehdi SM Sajjadi, Jonathan T Barron, Alexey Dosovitskiy, and Daniel Duckworth. Nerf in the wild: Neural radiance fields for unconstrained photo collections. In *Proceedings of the IEEE/CVF conference on computer vision and pattern recognition*, pages 7210–7219, 2021. 2, 3
- [34] Ben Mildenhall, Pratul P Srinivasan, Matthew Tancik, Jonathan T Barron, Ravi Ramamoorthi, and Ren Ng. Nerf: Representing scenes as neural radiance fields for view synthesis. In *European Conference on Computer Vision*, pages 405–421. Springer, 2020. 2, 3
- [35] Daniel Müllner. Modern hierarchical, agglomerative clustering algorithms. *arXiv preprint arXiv:1109.2378*, 2011. 4, 1
- [36] Maxime Oquab, Timothée Darcet, Théo Moutakanni, Huy Vo, Marc Szafraniec, Vasil Khalidov, Pierre Fernandez, Daniel Haziza, Francisco Massa, Alaaeldin El-Nouby, et al. Dinov2: Learning robust visual features without supervision. *arXiv preprint arXiv:2304.07193*, 2023. 3, 5, 7, 8, 1
- [37] Wongi Park, Myeongseok Nam, Siwon Kim, Sangwook Jo, and Soomok Lee. Forestsplats: Deformable transient field for gaussian splatting in the wild. *arXiv preprint arXiv:2503.06179*, 2025. 2, 3, 1
- [38] Nikhila Ravi, Valentin Gabeur, Yuan-Ting Hu, Ronghang Hu, Chaitanya Ryali, Tengyu Ma, Haitham Khedr, Roman Rädle, Chloe Rolland, Laura Gustafson, et al. Sam 2: Segment anything in images and videos. *arXiv preprint arXiv:2408.00714*, 2024. 3, 4, 8, 1
- [39] Konstantinos Rematas, Andrew Liu, Pratul P Srinivasan, Jonathan T Barron, Andrea Tagliasacchi, Thomas Funkhouser, and Vittorio Ferrari. Urban radiance fields. In *Proceedings of the IEEE/CVF Conference on Computer Vision and Pattern Recognition*, pages 12932–12942, 2022. 2
- [40] Weining Ren, Zihan Zhu, Boyang Sun, Jiaqi Chen, Marc Pollefeys, and Songyou Peng. Nerf on-the-go: Exploiting uncertainty for distractor-free nerfs in the wild. In *Proceedings of the IEEE/CVF Conference on Computer Vision and Pattern Recognition*, pages 8931–8940, 2024. 2, 3, 6, 7, 8
- [41] Robin Rombach, Andreas Blattmann, Dominik Lorenz, Patrick Esser, and Björn Ommer. High-resolution image synthesis with latent diffusion models. In *Proceedings of the IEEE/CVF conference on computer vision and pattern recognition*, pages 10684–10695, 2022. 3, 8, 1
- [42] Sara Sabour, Suhani Vora, Daniel Duckworth, Ivan Krasin, David J Fleet, and Andrea Tagliasacchi. Robustnerf: Ignoring distractors with robust losses. In *Proceedings of the IEEE/CVF Conference on Computer Vision and Pattern Recognition*, pages 20626–20636, 2023. 2, 3, 4, 6, 7
- [43] Sara Sabour, Lily Goli, George Kopanas, Mark Matthews, Dmitry Lagun, Leonidas Guibas, Alec Jacobson, David J Fleet, and Andrea Tagliasacchi. Spotlessplats: Ignoring distractors in 3d gaussian splatting. *arXiv preprint arXiv:2406.20055*, 2024. 1, 2, 3, 6, 7, 8, 5
- [44] Nicolas Schischka, Hannah Schieber, Mert Asim Karaoglu, Melih Gorgulu, Florian Grötzner, Alexander Ladikos, Nassir Navab, Daniel Roth, and Benjamin Busam. Dynamon: Motion-aware fast and robust camera localization for dynamic neural radiance fields. *IEEE Robotics and Automation Letters*, 2024. 2
- [45] Karen Simonyan and Andrew Zisserman. Very deep convolutional networks for large-scale image recognition. *arXiv preprint arXiv:1409.1556*, 2014. 7, 1
- [46] Hwanjun Song, Minseok Kim, Dongmin Park, Yooju Shin, and Jae-Gil Lee. Learning from noisy labels with deep neural networks: A survey. *IEEE transactions on neural networks and learning systems*, 34(11):8135–8153, 2022. 2
- [47] Jiaming Sun, Xi Chen, Qianqian Wang, Zhengqi Li, Hadar Averbuch-Elor, XiaoWei Zhou, and Noah Snavely. Neural 3d reconstruction in the wild. In *ACM SIGGRAPH 2022 conference proceedings*, pages 1–9, 2022. 2
- [48] Matthew Tancik, Vincent Casser, Xinchen Yan, Sabeek Pradhan, Ben Mildenhall, Pratul P Srinivasan, Jonathan T Barron, and Henrik Kretzschmar. Block-nerf: Scalable large scene neural view synthesis. In *Proceedings of the IEEE/CVF conference on computer vision and pattern recognition*, pages 8248–8258, 2022. 2
- [49] Luming Tang, Menglin Jia, Qianqian Wang, Cheng Perng Phoo, and Bharath Hariharan. Emergent correspondence from image diffusion. *Advances in Neural Information Processing Systems*, 36:1363–1389, 2023. 3, 4, 8, 1
- [50] Haithem Turki, Deva Ramanan, and Mahadev Satyanarayanan. Mega-nerf: Scalable construction of large-scale nerfs for virtual fly-throughs. In *Proceedings of the IEEE/CVF conference on computer vision and pattern recognition*, pages 12922–12931, 2022. 2
- [51] Paul Ungermann, Armin Ettenhofer, Matthias Nießner, and Barbara Rössle. Robust 3d gaussian splatting for novel

- view synthesis in presence of distractors. *arXiv preprint arXiv:2408.11697*, 2024. [2](#)
- [52] Michael Van den Bergh, Xavier Boix, Gemma Roig, and Luc Van Gool. Seeds: Superpixels extracted via energy-driven sampling. *International Journal of Computer Vision*, 111: 298–314, 2015. [4](#), [8](#), [1](#)
- [53] Yihao Wang, Marcus Klasson, Matias Turkulainen, Shuzhe Wang, Juho Kannala, and Arno Solin. Desplat: Decomposed gaussian splatting for distractor-free rendering. *arXiv preprint arXiv:2411.19756*, 2024. [2](#)
- [54] Yukun Wang, Kunhong Li, Minglin Chen, Longguang Wang, Shunbo Zhou, Kaiwen Xue, and Yulan Guo. Distractor-free novel view synthesis via exploiting memorization effect in optimization. In *European Conference on Computer Vision*, pages 477–493. Springer, 2024. [2](#), [4](#), [5](#), [6](#), [7](#), [8](#)
- [55] Yuze Wang, Junyi Wang, and Yue Qi. We-gs: An in-the-wild efficient 3d gaussian representation for unconstrained photo collections. *arXiv preprint arXiv:2406.02407*, 2024. [2](#)
- [56] Zhou Wang, Alan C Bovik, Hamid R Sheikh, and Eero P Simoncelli. Image quality assessment: from error visibility to structural similarity. *IEEE transactions on image processing*, 13(4):600–612, 2004. [8](#)
- [57] Guanjun Wu, Taoran Yi, Jiemin Fang, Lingxi Xie, Xiaopeng Zhang, Wei Wei, Wenyu Liu, Qi Tian, and Xinggang Wang. 4d gaussian splatting for real-time dynamic scene rendering. In *Proceedings of the IEEE/CVF conference on computer vision and pattern recognition*, pages 20310–20320, 2024. [2](#)
- [58] Congrong Xu, Justin Kerr, and Angjoo Kanazawa. Splatfacto-w: A nerfstudio implementation of gaussian splatting for unconstrained photo collections. *arXiv preprint arXiv:2407.12306*, 2024. [2](#)
- [59] Yifan Yang, Shuhai Zhang, Zixiong Huang, Yubing Zhang, and Mingkui Tan. Cross-ray neural radiance fields for novel-view synthesis from unconstrained image collections. In *Proceedings of the IEEE/CVF International Conference on Computer Vision*, pages 15901–15911, 2023. [2](#)
- [60] Zeyu Yang, Hongye Yang, Zijie Pan, and Li Zhang. Real-time photorealistic dynamic scene representation and rendering with 4d gaussian splatting. *arXiv preprint arXiv:2310.10642*, 2023. [2](#)
- [61] Ziyi Yang, Xinyu Gao, Wen Zhou, Shaohui Jiao, Yuqing Zhang, and Xiaogang Jin. Deformable 3d gaussians for high-fidelity monocular dynamic scene reconstruction. In *Proceedings of the IEEE/CVF conference on computer vision and pattern recognition*, pages 20331–20341, 2024. [2](#)
- [62] Vickie Ye, Ruilong Li, Justin Kerr, Matias Turkulainen, Brent Yi, Zhuoyang Pan, Otto Seiskari, Jianbo Ye, Jeffrey Hu, Matthew Tancik, and Angjoo Kanazawa. gsplat: An open-source library for Gaussian splatting. *arXiv preprint arXiv:2409.06765*, 2024. [7](#), [1](#)
- [63] Zehao Yu, Anpei Chen, Binbin Huang, Torsten Sattler, and Andreas Geiger. Mip-splatting: Alias-free 3d gaussian splatting. In *Proceedings of the IEEE/CVF conference on computer vision and pattern recognition*, pages 19447–19456, 2024. [1](#)
- [64] Dongbin Zhang, Chuming Wang, Weitao Wang, Peihao Li, Minghan Qin, and Haoqian Wang. Gaussian in the wild: 3d gaussian splatting for unconstrained image collections. In *European Conference on Computer Vision*, pages 341–359. Springer, 2024. [2](#)
- [65] Richard Zhang, Phillip Isola, Alexei A Efros, Eli Shechtman, and Oliver Wang. The unreasonable effectiveness of deep features as a perceptual metric. In *Proceedings of the IEEE conference on computer vision and pattern recognition*, pages 586–595, 2018. [8](#), [1](#)

# 3DGS-HPC: Distractor-free 3D Gaussian Splatting with Hybrid Patch-wise Classification

## Supplementary Material

Table 1. Settings for Our Perceptual Error Metrics.

Vision Model	Extracted Feature Layers
VGG-16 [45]	{conv1_2, conv2_2, conv3_3, conv4_3, conv5_3}
ResNet-18 [16]	{layer1, layer2, layer3, layer4}
DINOv2 ViT-S/14 [36]	{layer2, layer5, layer8, layer11}

Table 2. Performance of Our Patch-wise Classification vs. Its Refinement Variant. Our method can significantly reduce training time and have slightly better performance in visual metrics.

	RobustNeRF (Avg.)				On-the-go (Avg.)			
	PSNR $\uparrow$	SSIM $\uparrow$	LPIPS $\downarrow$	Train hrs. $\downarrow$	PSNR $\uparrow$	SSIM $\uparrow$	LPIPS $\downarrow$	Train hrs. $\downarrow$
(a) Refinement Variant	29.74	.912	.074	2.53	23.69	.848	.111	2.09
(b) Ours	<b>29.81</b>	<b>.913</b>	<b>.074</b>	<b>0.22</b>	<b>23.86</b>	<b>.849</b>	<b>.106</b>	<b>0.25</b>

## 7. Implementation & Experimental Details

**3DGS.** As mentioned in Sec. 5.1 of the main paper, we develop our model based on the open-source codebase gsplat [62], which reproduces native 3DGS [19] and aligns its performance. We follow the same training settings and adaptive density control strategy as the native model, except that we do not remove large-scale Gaussians during periodic pruning, which would otherwise result in some scene backgrounds represented by large-scale Gaussians having degraded geometry and appearance. All experiments of our method are conducted on an NVIDIA RTX 4090 GPU.

**Update of Static Maps.** Similar to prior works [22, 32], we do not apply or update static maps in the first 500 steps to warm up the 3DGS optimization and ensure the initialization of the scene reconstruction. We then apply static maps in the remaining steps and update them every 100 steps by rendering all training images with the current 3DGS. Since 3DGS resets the opacity every 3,000 steps during training, we only apply but do not update static maps within 200 steps after each opacity reset.

**Perceptual Error Metrics.** Inspired by LPIPS [65], we implement our perceptual metrics by extracting multi-layer features from vision foundation models. Since feature maps from different layers have varying spatial resolutions, we first compute cosine error maps at each layer and then up-sample them to the input resolution using bilinear interpolation. The final error map is obtained by averaging these aligned maps. The vision models and their specific layers used for feature extraction are summarized in Tab. 1.

**Partitioning Strategies.** We implement different partitioning strategies for comparison:

- *Superpixel.* Following ForestSplats [37], we leverage the superpixel algorithm SEEDS [52] from the OpenCV li-

Table 3. Quantitative Efficiency Comparisons between Different Methods. Our method outperforms most other methods in training time and memory usage.

	Avg. Train Time (min) $\downarrow$	Avg. GPU Mem (GB) $\downarrow$
SLS-mlp [43]	11.91	3.60
WildGaussians [22]	24.10	16.02
T-3DGS [32]	26.75	4.36
Ours (VGG)	16.35	2.09
Ours (ResNet)	13.29	1.98
Ours (DINOv2)	17.52	2.05

brary and set the superpixel number of each image to 100 by default.

- *SAM2.* The Segment Anything Model 2 (SAM2) [38] is a foundation model extended from SAM [21] for promptable visual segmentation in images and videos. Following NeRF-HuGS [6], we take a regular point grid with a resolution of  $64 \times 64$  as input prompt to generate instance masks for each training image.
- *Feature Clustering.* Following SpotLessSplats [43], we execute agglomerative clustering [35] on the feature map from the 2nd upsampling layer of Stable Diffusion v2.1 [41, 49], and set the cluster number of each image to 100 by default.

## 8. Additional Experiments

### 8.1. Path-wise Classification Implementation

In Sec. 4.1 of the main paper, we propose to classify patches directly based on their average errors rather than using them to refine results after per-pixel classification. As shown in Tab. 2, when the patch size is set to 16, our proposed method significantly reduces training time due to the reduction in the number of classification samples and performs slightly better in visual metrics. We therefore uniformly use our proposed patch-wise classification implementation in other experiments for efficiency.

### 8.2. Efficiency Comparisons of Different Methods

As shown in Tab. 3, we additionally provide quantitative efficiency comparisons of different methods across all the scenes used in the main paper. Specifically, SLS-mlp [43] uses semantic priors as model input, while WildGaussians [22] and T-3DGS [32] utilize perceptual error metrics. Compared to these methods, Ours (ResNet) achieves the smallest GPU memory usage and is only slower than SLS-mlp in average training time.

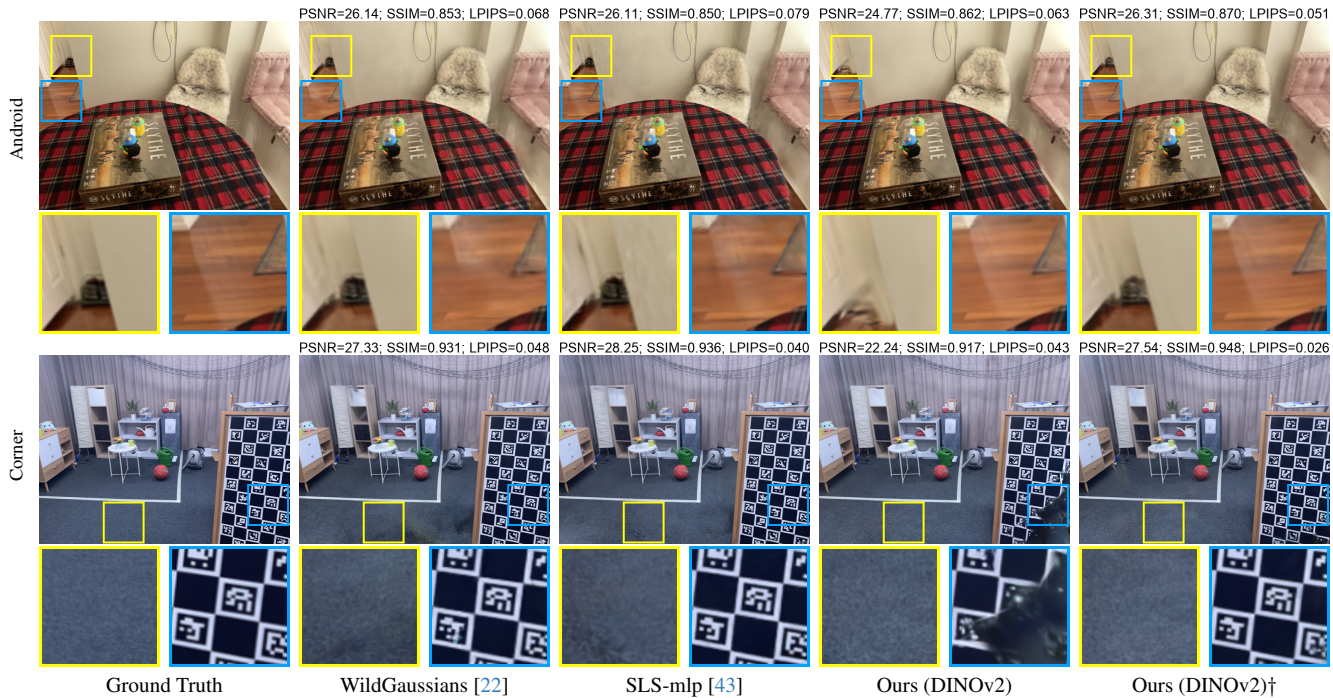


Figure 10. **Comparisons on Challenging Cases.** Our method achieves better visual quality in most regions (e.g., walls and floors) with default settings, while it can further capture frequently occluded details (e.g., shoes and plaid patterns) by increasing warm-up steps ( $\dagger$ ).

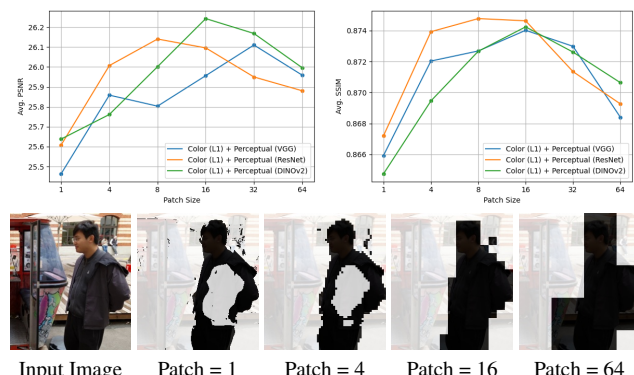


Figure 11. **Performance of Different Patch Sizes.** Patch sizes that are extremely small ( $< 8$ ) or large ( $> 16$ ) will lead to suboptimal quantitative results, and the resulting mask will fail to accurately label and filter out transient distractors (e.g., people).

### 8.3. More Results on Android & Corner Scenes

As shown in Figs. 6 and 7 of the main paper, our method outperforms previous methods in most visual metrics across various scenes. However, it brings less improvement in PSNR on Android and Corner scenes compared to others. We ascribe this to a longstanding challenge in distractor-free NeRF/3DGS methods: the inherent ambiguity between infrequently observed static objects and genuinely transient ones. Since transient objects are typically identified based on reconstruction errors arising from their limited presence in the training images, rarely visible static content may be

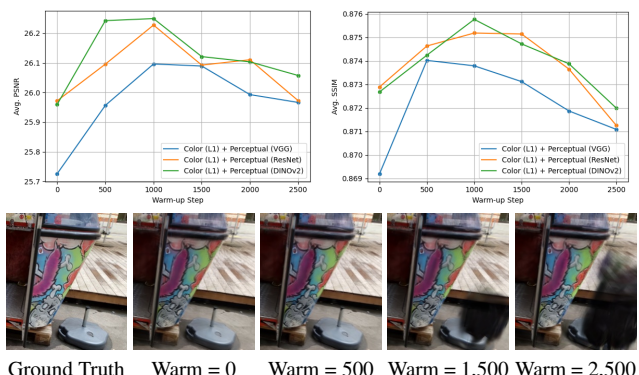


Figure 12. **Performance of Different Warm-up Steps.** When the number of warm-up steps exceeds 1,000, the model is at risk of “memorizing” transient distractors, leading to artifacts in the rendered results.

mistakenly classified as transient. Nevertheless, our method can mitigate this issue and improve PSNR by straightforward hyperparameter tuning (i.e., the warm-up steps) to preserve more static details (Fig. 10). Please see Fig. 15 for additional qualitative results.

### 8.4. Choice of Hyperparameters

Our method has two key hyperparameters: i) the patch size for the patch-wise partitioning strategy, and ii) the warm-up step in the 3DGS optimization process. Following the main paper, we conduct experiments to investigate their choices.

Method	Brandenburg Gate			Sacre Coeur			Trevi Fountain			Avg.		
	PSNR $\uparrow$	SSIM $\uparrow$	LPIPS $\downarrow$	PSNR $\uparrow$	SSIM $\uparrow$	LPIPS $\downarrow$	PSNR $\uparrow$	SSIM $\uparrow$	LPIPS $\downarrow$	PSNR $\uparrow$	SSIM $\uparrow$	LPIPS $\downarrow$
3DGS [19]	21.20	.889	.131	16.73	.833	.166	17.66	.729	.210	18.53	.817	.169
NeRF-HuGS [6]	24.69	.890	.132	21.09	.819	.169	22.63	.748	.195	22.80	.819	.165
WildGaussians [22]	27.77	.927	.133	22.56	.859	.177	23.63	.766	.228	24.65	.851	.179
Ours	20.76	.879	.139	16.56	.822	.177	17.31	.691	.261	18.21	.797	.193
Ours w/ Embed.	27.90	.932	.094	22.68	.873	.126	22.35	.785	.176	24.31	.863	.132



Figure 13. **Comparisons on the Phototourism Dataset [33].** The first, second, and third best values are highlighted. Our extended method can easily adapt to scenes with appearance variations by assigning learnable embeddings to each image and Gaussian.



Figure 14. **A Failure Case.** Without prior knowledge from the generative model, 3DGS and its variants cannot correctly predict the scene content that has never been observed before.

**Patch Size.** As shown in Fig. 11, the average PSNRs and SSIMs of our method using different perceptual error metrics first increase and then decrease as the patch size gradually increases on both the RobustNeRF and On-the-go datasets. This indicates that the best batch size is achieved by striking a balance between maintaining local spatial consistency and flexibly representing transient distractors. Nevertheless, our method consistently achieves better performance than pixel-wise classification (*i.e.*, Patch Size = 1) even without carefully choosing the patch size, consistent with the results of ablation studies (Sec. 5.3).

**Warm-up Step.** The warm-up phase aims to prevent static details from being excessively removed during early training, as the model will underfit the scene and have large errors when initialized. As shown in Fig. 12, the use of too few warm-up steps often degrades performance as it unnecessarily removes static details, while the use of too many steps causes 3DGS to overfit to transient distractors. We therefore set the default warm-up step to 500.

### 8.5. Extension to Scenes w/ Appearance Variations

Our method is designed for scenes with stable appearances, but can extend naturally to non-static appearances caused by diverse shooting environments and shooting equipment (*e.g.*, different weather changes or inconsistent

white balances). Specifically, we apply a widely adopted paradigm [6, 22, 33] to our method, which assigns learnable appearance embeddings to each image and Gaussian. When rendering a specific image, each Gaussian embedding is combined with the image embedding and processed by a lightweight MLP, thereby scaling and biasing the corresponding Gaussian colors to achieve color changes.

We conduct an experiment on the Phototourism Dataset [33], which includes three scenes of cultural landmarks with varying appearances and various distractors. As shown in Fig. 13, our extended method can capture appearance variations compared to the original method, and achieves quantitative performance comparable to previous baseline methods, leading in SSIM and LPIPS metrics. In terms of visual quality, our extended method effectively reduces artifacts caused by appearance variations compared to the original method, resulting in cleaner rendered results.

## 9. Limitations and Future Work

As mentioned above, despite the superiority of our method, it still faces a longstanding challenge in distractor-free NeRF/3DGS: reliably distinguishing between transient distractors and infrequently visible static elements. These static elements can be highly reflective objects whose appearance changes drastically under limited views (*e.g.*, the

ground reflection in Fig. 10), or objects that are rarely observed (*e.g.*, black shoes in Fig. 10). In such cases, these static regions may be mistakenly treated as transient elements due to insufficient visibility. Therefore, as long as the reconstruction error remains the primary criterion for distinguishing transients, this challenge is likely to persist. Addressing it may require a paradigm shift that could offer substantial benefits to the community. In addition, our method inherits the limitations of native 3DGS and its variants, particularly the inability to reconstruct unobserved scene content (Fig. 14). Future work may address this limitation by incorporating pre-trained generative models.

## **10. Additional Qualitative Results**

### **10.1. Evaluation on Novel View Synthesis**

We provide more qualitative results of view synthesis on different datasets. As shown in Fig. 15, existing methods exhibit limitations in managing transient distractors, while our method effectively balances the exclusion of transient distractors and retention of static details, thereby enhancing the rendering quality. Please zoom in for better details.

### **10.2. Evaluation on Static Map Generation**

We also provide more qualitative results of static maps. As shown in Figs. 16 and 17, existing methods that leverage semantic priors still exhibit limited efficacy in separating transient distractors from static backgrounds. Conversely, our proposed framework can generate more accurate static maps by addressing the inherent limitations of semantics.



Figure 15. Qualitative Results of View Synthesis on Different Datasets.



Figure 16. Qualitative Results of Static Map Generation on the RobustNeRF Dataset.



Figure 17. Qualitative Results of Static Map Generation on the On-the-go Dataset.